Compact FBG diaphragm accelerometer based on L-shaped rigid cantilever beam

Yinyan Weng (翁银燕)[1*]**, Xueguang Qiao (乔学光)**[1,2]**, Zhongyao Feng (冯忠耀)**[1]**,**

Manli Hu (忽满利)[1]**, Jinghua Zhang (张敬花)**[1]**, and YangYang (杨 扬)**[1]

[1]*Department of Physics, Northwest University of China, Xi'an 710069, China*

[2]*Key Laboratory of Photoelectricity Gas-Oil Logging and Detecting, Ministry of Education,*

Xi'an Shiyou University of China, Xi'an 710065, China

Corresponding author: wyyandlym@163.com

Received March 4, 2011; accepted April 21, 2011; posted online July 11, 2011

A compact fiber Bragg grating (FBG) diaphragm accelerometer based on L-shaped rigid cantilever beam is proposed and experimentally demonstrated. The sensing system is based on the integration of a flat diaphragm and an L-shaped rigid cantilever beam. The FBG is pre-tensioned and the two side points are fixed, efficiently avoiding the unwanted chirp effect of grating. Dynamic vibration measurement shows that the proposed FBG diaphragm accelerometer provides a wide frequency response range (0–110 Hz) and an extremely high sensitivity (106.5 pm/g), identifying it as a good candidate for embedding structural health monitoring and seismic wave measurement.

OCIS codes: 060.2370, 060.3735, 280.4788.

doi: 10.3788/COL201109.100604.

In the past few decades, accelerometers based on fiber Bragg grating (FBG) have attracted a great deal of interest from researchers and engineers because they play a vital role in vibration measurements. In recent years, FBG accelerometers have been more and more applied in structural health monitoring[1−3] and seismic wave measurement[4−6]. This study concerns about the development of geophones composed of FBG accelerometers in seismic exploration. The main frequency of geophones in seismic wave measurement of oil and gas exploration is usually below 100 Hz. An FBG-based accelerometer consisting of a mass resting on a layer of compliant material supported by a rigid base plate was proposed by Berkoff *et al.*[7]. The natural frequency of the acceleration sensor is approximately 2 000 Hz, while the overall sensitivity is predicted to be about 135.32 pm/g. However, it suffers the disadvantage of susceptibility to cross-axis excitation because of the embedded FBG. Then, a good performance horizontal vibration FBG accelerometer based on cantilever beam was reported by Au *et al.*[8]. The accelerometer can catch up the maximum input signal frequency of up to 150 Hz, but it has a low sensitivity of 22.89 pm/g. Recently, Nan *et al.* presented a FBG vibration sensor using a double-cantilever beam structure[9]. Experimental results show that it has a narrow frequency resonance range between 0.1 and 15 Hz with a high sensitivity of 189 mV/g.

In this letter, we report the design and performance of a novel diaphragm accelerometer. It integrates a flat diaphragm and an L-shaped rigid cantilever beam, which widens the range of frequency response and enhances the sensitivity coefficient. Experimental results demonstrate that this sensor provides an extremely high sensitivity up to 106.5 pm/g and a flat frequency response ranging from 0 to 110 Hz, which can cover the major frequencies to be measured in seismic wave measurement. Moreover, in this structure, another function of the flat diaphragm is to minimize cross-axis sensitivity.

The structural schematic of the diaphragm accelerometer is shown in Fig. 1. The rigid cantilever beam was made into an L-shaped lever, which can rotate around the precision bearing flexibly. The diaphragm's two side edges were clamped by two locking pillars. An FBG was glued between point *A* of the lever and point *B* of the shell. The FBG was pre-tensioned and the two side points were fixed, which can effectively prevent the chirping of grating. The mass of the brass consisting of three parts functions as a connection between the lever and the diaphragm. The above mass was made into a bolt, the below mass was made into a locking nut, and the middle mass was used as counter weight.

The mechanical model can be simplified into a single degree of freedom mass-spring system with no damping under the premise that the mass of the diaphragm is much smaller than that of the brass. When this structure is subjected to an acceleration along vertical direction, the inertial force of mass *F* will give rise to the deflection of the center of the diaphragm and the tensioning or compression of the FBG due to the rotation of the lever. The strain force of FBG *T* will bring about a reaction force to the diaphragm through the lever, which also results in the deflection of the center of the diaphragm.

The spring stiffness of the FBG is represented by

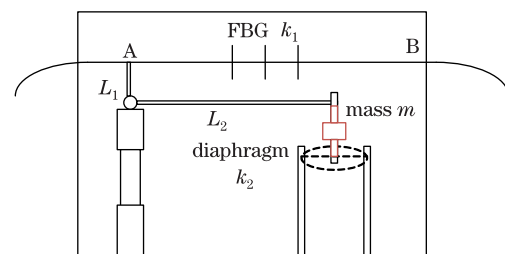$$k_1 = \frac{E_{\rm f} A_{\rm f}}{L}, \tag{1}$$

Fig. 1. Structural schematic of the diaphragm accelerometer.

where E_f and A_f are the elastic modulus and the cross-section area of the fiber, respectively, and L is the distance between points A and B.

The bending rigidity of the diaphragm is represented as

$$D = \frac{Et^3}{12(1-\mu^2)},\qquad(2)$$

where E and μ are the Young's modulus and Poisson's ratio of the diaphragm, respectively, and t is the thickness of the diaphragm. The numerical coefficient is defined as

$$A_s = 1 - \left(\frac{r}{R}\right)^2 - \frac{4\ln^2\left(\frac{R}{r}\right)}{\left(\frac{R}{r}\right)^2-1},\qquad(3)$$

where R and r are the radius and contract radius of the diaphragm, respectively. According to elastic knowledge[10], the deflection of the center of the diaphragm caused by the inertial force of mass F is given by

$$\omega_F = \frac{A_s R^2}{16\pi D}F.\qquad(4)$$

Meanwhile, the deflection of the center of the diaphragm caused by the reaction force resulting from the force of FBG T is given as

$$\omega_T = \frac{A_s R^2}{16\pi D}\frac{L_1}{L_2}T = \frac{A_s R^2}{16\pi D}\frac{L_1}{L_2}E_f A_f \varepsilon,\qquad(5)$$

where L_1 and L_2 are the lengths of the short arm and long arm of the lever, respectively. ε is the strain value.

Hence, the actual deflection of the center of the diaphragm can be expressed as

$$\omega = \omega_F - \omega_T = \frac{A_s R^2}{16\pi D}\left(F - \frac{L_1}{L_2}E_f A_f \varepsilon\right).\qquad(6)$$

According to geometric knowledge, the relationship between strain ε and deflection ω can be expressed as

$$\varepsilon = \frac{L_1}{LL_2}\omega = \frac{L_1}{LL_2}\frac{A_s R^2}{16\pi D}\left(F - \frac{L_1}{L_2}E_f A_f \varepsilon\right).\qquad(7)$$

Thus, strain ε can be described as

$$\varepsilon = \frac{L_1 L_2 A_s R^2}{16\pi D L_2^2 L + E_f A_f A_s L_1^2 R^2}F.\qquad(8)$$

Therefore, sensitivity coefficient S can be represented by

$$S = \frac{\Delta\lambda}{a} = (1-P_e)\lambda\frac{mL_1 L_2 A_s R^2}{16\pi D L_2^2 L + E_f A_f A_s L_1^2 R^2}.\qquad(9)$$

According to the equation of motion of the structure, natural frequency can be expressed as

$$f = \frac{1}{2\pi}\sqrt{\frac{k}{m}} = \frac{1}{2\pi}\sqrt{\frac{k_2 + (\frac{L_1}{L_2})^2 k_1}{m}},\qquad(10)$$

where m is the total mass of the brass.

The parameters of the diaphragm accelerometer are listed in Table 1. The sensor provides a natural frequency f=176.24 Hz and sensitivity coefficient S=109.15 pm/g.

The experimental setup of the accelerometer is shown in Fig. 2. A standard charge acceleration sensor was attached above the accelerometer to make sure that the vibration was the same. In the experiment, we used a small precision shaking table (JZ-40, Beijing Wave Spectrum, China) to provide some sine excitation as the input signal and a fiber grating sensing interrogator (SM 130 American Micron Optics, USA) with resolution of 1 pm and sampling frequency of 1 000 Hz to deal with the output sine wave signal. The experiment included an amplitude-frequency characteristic test and a sensitivity test. We ignored the influence of temperature to the FBG because it was considered to be constant in the whole dynamic experiments.

From a practical point of view, the wider the frequency response range of the accelerometer, the better the test results. In this experiment, the sine excitation frequency was increased from 10 to 400 Hz with the same acceleration of approximately 0.5 g. We used the dynamic demodulator to obtain the sine output of every frequency and then found the peak-to-peak wavelength amplitude shift as the sensor output in order to determine the frequency response range. The amplitude frequency characteristic of the diaphragm accelerometer is shown in Fig. 3. From the figure, we can see clearly that the resonant frequency is about 220 Hz and that there is a flat frequency response between 0 and 110 Hz,

Table 1. Parameters of the Diaphragm Accelerometer

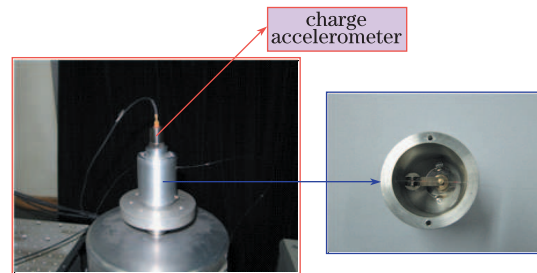| Parameter	Value
L_1 (mm)	5
L_2 (mm)	15
L (mm)	30
R (mm)	10
r (mm)	2
t (mm)	0.05
μ	0.3
m (g)	4.5
λ (nm)	1 538.31
E (GPa)	200
E_f (GPa)	73
A_f (m^2)	1.227$\times10^{-8}$

Fig. 2. Experimental setup of the diaphragm accelerometer.

which is wider than expected. This is largely due to the integration of an L-shaped rigid cantilever beam and a flat diaphragm. This frequency range can undoubtedly cover the key frequencies to be measured in seismic wave exploration.

The higher the sensitivity of the accelerometer, the stronger the ability to acquire the weak vibration signal. In this experiment, the amplitude of sine excitation acceleration was increased from 1.5 to 15 m/s^2 with a constant acceleration of approximately 50 Hz. We also used the dynamic demodulator to obtain the sine output of every frequency and then found the peak-to-peak wavelength amplitude shift as the sensor output in order to determine sensitivity. The linear relationship between the peak-to-peak wavelength shift and acceleration is shown in Fig. 4.

The test result shows that the sensitivity coefficient is about 106.5 pm/g, which is in good agreement with theoretical analysis. When the input frequency remains at 50 Hz, the accelerometer real-time output response is shown in Fig. 5 with the input signal acceleration at 5.5 and 8.5 m/s^2. When the input frequency remains at 100 Hz, the accelerometer real-time output response is shown in Fig. 6 with the input signal at 4.5 and 5.5 m/s^2. It can be seen that the diaphragm accelerometer can acquire a more perfect sine wave with the signal frequency of 50 Hz than of 100 Hz. In addition, the waveforms of sine output show that the grating is not chirped during the experiment.

Cross-axis response is a crucial characteristic of a single-freedom vibration accelerometer. In the process of the experiment, the sine excitation of about 1 g acceleration is respectively exerted to the accelerometer in the main-axis direction and cross-axis direction with 190-Hz frequency. Figure 7 presents the time curve showing the vibration performance of the main axis and the cross axis. The amplitude of the main-axis vibration is
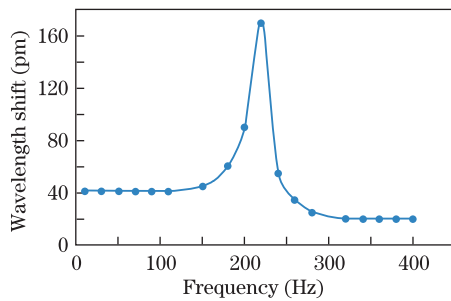
118.5 pm, while the amplitude of the cross-axis vibration is 2.5 pm. Therefore, the interference degree is 2.11%, indicating that this design of the accelerometer is valid for cross-axis anti-interference.

Fig. 5. Accelerometer real-time output response with the signal frequency at 50 Hz and acceleration at (a) 5.5 and (b) 8.5 m/s^2.

Fig. 6. Accelerometer real-time output response with the signal frequency at 100 Hz and acceleration at (a) 4.5 and (b) 5.5 m/s^2.

Fig. 3. Amplitude-frequency characteristic of the diaphragm sensor.
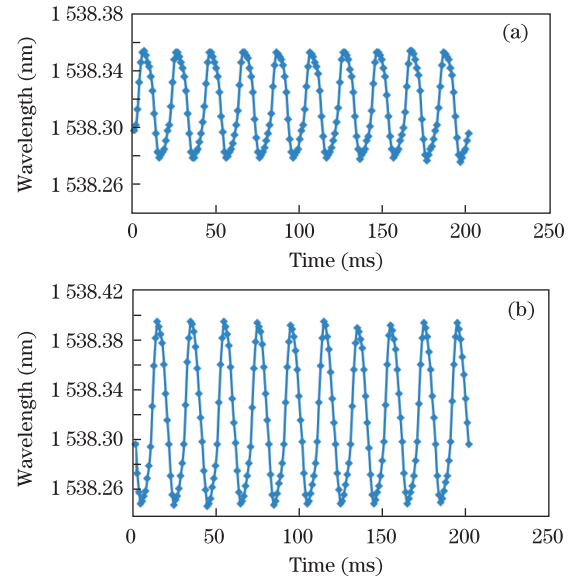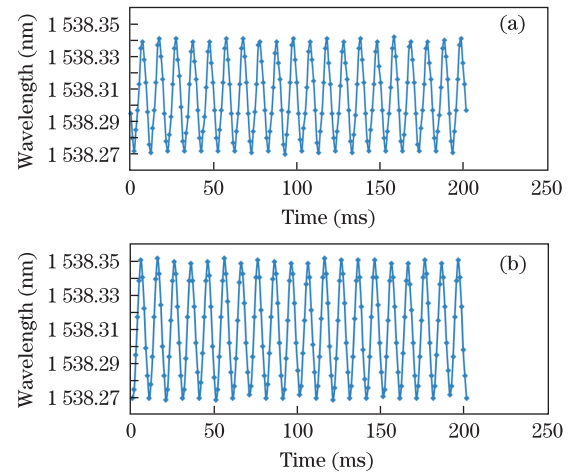

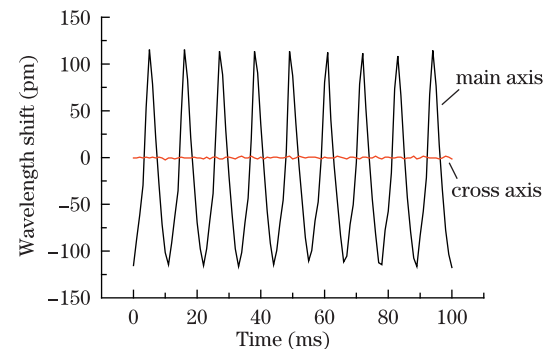Fig. 4. Linear response of peak-to-peak wavelength shift versus acceleration.

Fig. 7. Characteristic of cross-axis anti-interference.

In conclusion, the design of a novel FBG diaphragm accelerometer based on L-shaped rigid cantilever beam is proposed. Excellent performances have been achieved, including a wide frequency response range (0–110 Hz) and a high sensitivity (106.5 pm/g). Therefore, the frequency response range of this device is adapted for seismic exploration. Furthermore, the FBG is pre-tensioned and the two side points are fixed, efficiently preventing the unwanted chirp effect of grating. Moreover, the design of the accelerometer shows strong cross-axis anti-interference ability. To sum up, the proposed FBG accelerometer is a good candidate for real-time monitoring system in seismic wave measurement of oil and gas exploration.

References

1. L. Sun, Y. Shen, and C. Cao, Proc. SPIE **7292,** 729214 (2009).
2. P. F. da Costa Antunes, H. F. T. Lima, N. J. Alberto, H. Rodrigues, P. M. F. Pinto, J. de Lemos Pinto, R. N. Nogueira, H. Varum, A. G. Costa, and P. S. de Brito Andre, IEEE Sensors J. **9,** 1347 (2009).
3. F. Qin, H. Li, W. Fan, and Q. Sheng, Chin. Opt. Lett. **7,** 556 (2009).
4. Y. Zhang, S. Li, Z. Yin, B. Chen, and H. Cui, Opt. Eng. **45,** 084404 (2006).
5. A. Laudati, F. Mennella, M. Giordano, G. D'Altrui, C. Calisti Tassini, and A. Cusano, IEEE Photon. Technol. Lett. **19,** 1991 (2007).
6. W. Mo, H. Wu, D. Gao, and Z. Zhou, Chin. Opt. Lett. **7,** 798 (2009).
7. T. A. Berkoff and A. D. Kersey, IEEE Photon. Technol. Lett. **8,** 1677 (1996).
8. H. Y. Au, S. K. Khijwania, and H. Y. Tam, Proc. SPIE **7004,** 70042S (2008).
9. Q. Nan and C. Zou, in *Proceedings of Photonics and Optoelectronics* 1 (2009).
10. T. Stephen, *Theory of Plates and Shells* (McGraw-Hill, New York, 1959).